Convection Plasma Drifts in the Inner Magnetosphere Associated with a Plasmaspheric Drainage Plume

Chin. S. Lin[1], Huey-Ching Yeh[2], Bill R. Sandel[3], J. Goldstein[4], Frederick J. Rich[1], William J. Burke[1], and J. C. Foster[5]

Abstract

We report first observations of equatorial convection signatures associated with a plasmaspheric drainage plume using multi-satellite simultaneous observations. The Extreme Ultraviolet (EUV) sensor on board the IMAGE satellite observed a plume extending outward to L ≈ 2.8 near 16 - 17 magnetic local time (MLT) during the recovery phase of the 2000 Bastille Day magnetic storm. The plasmaspheric boundary was near L = 2 at other local times. We mapped simultaneously measured ionospheric plasma drifts from ROCSAT-1 and three Defense Meteorological Satellite Program (DMSP) spacecraft along magnetic field lines to infer ion convective velocities near the equatorial plane of the inner magnetosphere. The zonal component of convection derived from ROCSAT-1 ion-drift measurements manifests sharp positive azimuthal gradients in the vicinity of plume boundaries, reversing direction from westward to eastward. ROCSAT-1 also detected upward field-aligned flow, suggesting that plasmasphere refilling is associated with the sharp zonal velocity gradient. The meridional profile of horizontal velocities deduced from DMSP measurements shows a large flowing westward sub-auroral polarization stream (SAPS) located outside the plasmapause. The peak of SAPS was centered at about the radial distance of L= 2.8 with a full-width of about 1 R_E. In Earth's frame of reference, equatorial plasmas flow toward the plume from both the dayside and evening sides of the plume, suggesting a negative azimuthal gradient in the equatorial azimuthal velocity. The azimuthal velocity gradient was largest at the radial distance of the plume's outermost boundary. These observations provide new evidence about diversion of SAPS plasma flows and distinct signatures of azimuthal velocity reversal in the vicinity of plasmaspheric plumes.

[1] Air Force Research Laboratory Space Vehicles Directorate, Hanscom AFB, Massachusetts, USA.

[2] Institute of Space Science, National Central University, Jhongli, Taiwan.

[3] Lunar and Planetary Laboratory, University of Arizona, Tucson, Arizona, USA.

[4] Southwest Research Institute, San Antonio, Texas, USA.

[5] MIT Haystack Observatory, Westford, Massachusetts, USA.

1. Introduction

Plasmaspheric drainage plumes are generally believed to be byproducts of the plasmapause's inward motion during geomagnetic disturbances, a process known as plasmasphere erosion. Plasmaspheric dynamics are often described in terms of the superposed effects of convection, shielding and corotation [Grebowsky, 1970; Chen and Wolf, 1972; Spiro et al., 1981; Weiss et al., 1997; Lambour et al., 1997; Goldstein et al., 2004]. Cold plasma convective flow in the inner magnetosphere approximately follows equipotential lines. A superposition of stormtime dawn-to-dusk electric fields and co-rotational electric field causes equipotential lines to map radially outward and probably defines the bulged plasmaspheric boundary in the dusk sector [Chen and Wolf, 1972]. The build up of ring-current pressure during the main phase of a geomagnetic storm distorts the magnetic field, contributing to a pre-midnight plasmapause bulge. The asymmetric ring current also couples to the ionosphere via field-aligned currents to concentrate the westward flowing sub-auroral polarization streams (SAPS) that help to form plasmaspheric drainage plumes on the equatorial plane [Goldstein et al., 2003a; Mishin et al., 2003; Goldstein et al., 2004].

The overlap of SAPS convection with the outer portion of the drainage plumes was reported by Foster et al. [2002]. Foster et al. [2004] projected the plumes seen from the ground with GPS total electron content (TEC) observations onto the GSM equatorial plane via the Tsyganenko magnetic field model. They used this mapping to determine the erosion flux in the high-altitude region as due to flow from the plasmasphere into the dayside cusp. So far no direct plasma measurements have been reported that specify the radial and azimuthal distributions of equatorial plasma motion in and near plumes. Multi-satellite observations reported here help fill this gap. In this work, we use the Tsyganenko magnetic field model to obtain better radial profiles of plasmaspheric ion convection in the evening sector of the equatorial plane.

The Extreme Ultraviolet (EUV) sensor on the Imager for Magnetopause-to-Aurora Global Exploration (IMAGE) satellite provides global views of inner magnetospheric dynamics by imaging the distribution of resonantly-scattered 30.4-nm solar radiation by He^+ ions in the plasmasphere [Sandel et al., 2001]. The EUV effective lower threshold has been characterized during quiet or mildly disturbed intervals and is equivalent to about 30-50 electrons cm^{-3} [Goldstein et al, 2003b; Moldwin et al., 2003]. This threshold specifies 6-10 He^+ cm^{-3}, depending on the He^+/H^+ ratio. The retrieved images show plumes as narrow regions of enhanced He^+

density that connect to the main plasmasphere. Their typical sizes are 3-5 R_E in length and 0.5-1.0 R_E in width [Sandel et al. 2003]. The IMAGE EUV instrument observed persistent plume features from 0100 to 0600 UT on 16 July 2000, during the recovery phase of the Bastille Day magnetic storm. The images indicate that the plasmasphere was confined very close to Earth ($L \approx 2$). An example is shown in Figure 1.

While the drainage plume was being imaged, the ROCSAT-1 satellite, flying in a 35^o inclined orbit, detected unusual ion-convection signatures. Over the reported interval ROCSAT-1 was sampling L-shells between ~1.1 and 1.8. Three polar-orbiting spacecraft of the Defense Meteorological Satellite Program (DMSP F12, F13, and F15) simultaneously measured the cross-track (mostly east-west) component of ionospheric plasma drifts in the late-afternoon and early evening sectors. Observations from the three DMSP satellites thus provide complementary information about the radial profiles of convection related to the plasmaspheric plume in L shells between 1.5 and 4. They also provide information about the relative position of SAPS with respect to the plume and the plasmaspheric boundary.

Section 2 of this paper contains a brief description of procedures used to map ion drift velocities from the ionosphere to the equatorial plane. We then present simultaneous measurements from the ROCSAT-1, DMSP, and IMAGE satellites in Section 3. Observational results are summarized and discussed in Section 4. Section 5 gives the conclusion.

2. Data Sources and Methodology

The ROCSAT-1 satellite was launched in 1999 into a circular orbit at an altitude near 600 km and an inclination angle of 35^o. The Ionospheric Plasma and Electrodynamics Instrument (IPEI) payload contained an ion trap, two drift meters, and a retarding potential analyzer [Yeh et al., 1999] from which we deduce the two components of the convective velocity V_Z and V_M. V_Z is the zonal component, positive in the eastward direction; V_M is the radial component, positive in the outward direction [Lin and Yeh, 2005]. From these velocity components we calculate two components of convective electric fields E_M and E_Z at the satellite altitude, $\mathbf{E} = - \mathbf{V} \times \mathbf{B}$, where $\mathbf{V}$ and $\mathbf{B}$ are the convective magnetic field vectors at the satellite location. We then map the ionospheric electric field to the equatorial plane of the magnetosphere using the equipotential field-line assumption and relationships derived by Mozer [1970]

$$E_{Mi}h_i = E_{Me}h_e \quad (1)$$

and

$$E_{Zi}d_i = E_{Ze}d_e \quad (2)$$

Here h is the perpendicular distance between neighboring field lines in the meridional plane, and d is the distance perpendicular to the meridional plane between neighboring field lines. The subscripts i and e indicate locations in the ionosphere and at the equator, respectively. Finally, we calculate the equatorial convective velocity $\mathbf{V}_e = (\mathbf{E}_e \times \mathbf{B}_e)/B_e^2$. When we deduce equatorial convective velocity from the ROCSAT-1 data, we have determined the L value and the ratios of h_e/h_i, d_e/d_i, and B_e/B_i by tracing magnetic field lines from ROCSAT-1's position in the ionosphere to the equatorial plane using the IGRF magnetic field model.

Mozer, [1970] derived analytical expressions for mapping electric field components in a dipole magnetic field. Electric field components map along equipotential magnetic field lines between the ionosphere and the equatorial plane with ratios that depend on h_e/h_i and d_e/d_i, quantities that are functions of L. Since the L value of a magnetic field line defines the radial distance at which it crosses the equatorial plane, h_e is ΔL, the difference in L of two neighboring field lines in the equatorial plane. By requiring that ΔL for two neighboring field lines in the ionosphere is the same ΔL for the same two field lines in a meridional plane, the ratio of h_e/h_i can be shown to

$$h_e / h_i = \frac{1}{\sin\eta}\frac{\partial L}{\partial \lambda}\bigg|_{r=1} \quad (3)$$

where λthe magnetic latitude, r is is distance in units of earth radii, and η is the angle between the surface of the Earth and the magnetic field direction at the ionosphere. Similarly the ratio d_e/d_i is L/(r cos λ).

For the dipole magnetic field model, the equation of field line is simply r = L $\cos^2\lambda$. From Equation (3) and the equation of field line, we derive the ratio h_e/h_i to be

$$\frac{h_e}{h_i} = 2L(L-3/4)^{1/2} \quad (4)$$

Similarly, the ratio of d_e/d_i for the dipole file line is

$$\frac{d_e}{d_i} = L^{3/2} \quad (5)$$

By combining Equations (1) and (4) we obtain the ratios of zonal convective velocity between the equatorial plane and the ionosphere

$$\frac{V_{Ze}}{V_{Zi}} = \frac{E_{Me}B_i}{E_{Mi}B_e} = \frac{h_iB_i}{h_eB_e} = L^{3/2} \qquad (6)$$

Similarly from Equations (2) and (5) we obtain

$$\frac{V_{Me}}{V_{Mi}} = \frac{E_{Ze}B_i}{E_{Zi}B_e} = \frac{d_iB_i}{d_eB_e} = L(4L-3)^{1/2} \qquad (7)$$

DMSP satellites F12, F13, F14, and F15 measure the cross-track horizontal component of plasma velocity in the ionosphere. Because most DMSP measurements were acquired outside the plasmasphere, IGRF magnetic field model may not adequately account for the magnetic field inflation. Thus, when mapping the horizontal component of plasma velocity we used the magnetic field model of Tsyganenko [2002] to trace magnetic field lines from DMSP locations in the ionosphere to the equatorial plane. To distinguish from equatorial zonal velocity deduced from ROCSAT-1 data, we refer to the equatorial horizontal velocity determined from the DMSP data as equatorial azimuthal velocity.

We will follow the convention and present ROCSAT-1 and DMSP measurements of ion drift velocity in Earth's rotation frame by subtracting the co-rotational velocity. However, the EUV image represents ion density in the equatorial plane in Earth's inertial frame of reference. Furthermore, we have converted ionospheric drift velocity to the equatorial convective velocity, which is ordinarily expressed in the inertial frame as well. In order to conform to the convention, we include the co-rotational velocity in the presentation of equatorial convective velocity.

3. Observations

The peak intensity of the Bastille Day storm occurred at ~2200 UT on 15 July 2000 [Lin et al., 2001]. Recovery began on the beginning of 16 July. Due to the presence of intense solar-proton fluxes IMAGE failed to acquire clear EUV images before 16 July that might elucidate the plume's evolution during the main phase. However, the EUV imager detected plasmaspheric drainage plumes for four hours starting at ~ 0050 UT on 16 July. Figure 1a shows the EUV image at 0132 UT. The He^+ density boundary depends on the EUV sensitivity, which roughly defines a density boundary of about 50 cm^{-3}. Thus it is cautioned that the He^+ density boundary

investigated in this paper might differ from the hydrogen plasmaspheric boundary. During this severe Bastille Day magnetic storm, the EUV images show the dayside boundary close to 2 R_E with a plume protruding to ~ 2.8 R_E near 16.3 magnetic local time (MLT). In the evening sector, the He^+ plasmaspheric boundary reverted to ~2 R_E.

In Figures 1b we plot the He^+ density boundary from the EUV image by solid circles with plasma velocity vectors in the equatorial plane. The plasma velocity vectors are deduced from a complete orbit of ROCSAT-1 measurements after the removal of corotation. For this orbit, the L value sampled by ROCSAT-1 varies from 1.1 to 1.8. To promote interest in correlations between ROCSAT-1 observations and the plasmaspheric plume, we focus on the interval 0040 – 0216 UT. ROCSAT-1 acquired measurements near 16.3 MLT close in time to the 0132 UT EUV image. Figure 1b contains three lines: (1) A at ~15 MLT roughly corresponds to the place where the plasmaspheric bulge started, (2) B at ~16 MLT extends along the plume's dayside edge, and (3) C at ~ 19 MLT marks the plume's nightside edge. ROCSAT-1 data acquired near plume longitudes indicate that in the corotating frame of reference the equatorial convection was westward before 15 MLT and eastward after 16 MLT.

The top two panels of Figure 2 show the zonal and radial components of plasma velocity plotted respectively as a function of MLT for the same time interval as Figure 1b. Blue lines represent velocities measured by ROCSAT-1; red lines represent their mapping to the equatorial plane. Differences between velocities at ROCSAT-1's altitude (600 km) and the equatorial plane are small, because the decrease in magnetic field magnitude B is compensated by the increase in the E-field magnitude during mapping from the ionosphere to the equatorial plane (see Equations (6) and (7)). The top panel of Figure 2 indicates that the zonal velocity V_Z was nearly constant at about -250 m/s on the dayside. It increased sharply near 15 MLT (Line A), roughly matching the plume's sunward boundary (Line A in Figure 1b). The zonal velocity was near zero in the vicinity of the plume denoted by Line B. The plume's nightside boundary in the EUV image corresponds to the peak eastward zonal velocity, ~ 200 m/s (Line C in Figure 2). In association with the sharp V_Z gradient, a peak of upward field-aligned flow as high as 100 m/s was detected by ROCSAT-1 at 600 km altitude (third panel, Figure 2).

The radial component of velocity V_M was generally small (< 50 m/s) and outward between 12 and 21 MLT (middle panel, Figure 2). V_M also had a significant gradient between 15 and 16 MLT

(Lines A and B). The magnetic latitude of ROCSAT-1 at the plume's location happened to be near zero (bottom panel, Figure 2) and may account for a small negative V_M seen near 16 MLT.

Figure 3 displays the equatorial zonal velocity with corotation U_Z in Earth's inertial frame of reference (top panel) and its corresponding L values (bottom panel). Since the radial velocity in the inertial frame is the same as that presented in Figure 2, it is not repeated here. The horizontal dashed curve represents the corotation velocity in the equatorial plane at the radial distance of L. Figure 3 indicates that U_Z along ROCSAT-1's orbital trajectory was roughly constant and sub-corotational in the dayside from 05 to 15 MLT. Similar to V_Z, U_Z had a sharp positive azimuthal gradient of about 600 m/s/MLT between 15.5 and 16 MLT. From 16 to 03 MLT, equatorial plasma appeared to drift at supra-corotational speeds with minor variations. Thus, equatorial plasma zonal flow was sub-corotational before the plume's MLT (Line A) and became supra-corotation after it (Line B).

During the interval 0145–0210 UT, DMSP satellites measured ionospheric drifts at longitudes near the plasmaspheric plume. Figure 4 shows the EUV snapshot of the He^+ plasmaspheric acquired at 0202 UT and mapped to the equatorial plane in Geocentric Solar Magnetospheric (GSM) coordinate. For each pixel of the EUV image, the X, Y, and Z coordinates of points of minimum L along observing lines-of-sight from IMAGE were first computed, assuming a dipole field. These points were then mapped to the GSM equatorial plane (Z=0) using the magnetic field model of Tsyganenko [2002] calculated for the time of the observation. Figure 4 indicates that the plume's outer boundary remained at ~2.8 R_E. Similarly, the orbital tracks of three DMSP satellites (F12, F13, and F15) traversing the topside ionosphere near this EUV image time have been projected to the GSM Z=0 plane in order to give the best multi-instrument inter-comparison of the features observed. F13 passed through the plume's dayside edge along a trajectory from 17 MLT to 16.3 MLT as it moved from L = 1.5 (0145 UT) to L = 4 (0158 UT). Both F12 and F15 followed close trajectories passing outside the plume in the 20-21 MLT sector. F15 moved from the 20.6 MLT meridian at L = 1.5 (0159 UT) to the 20.3 MLT at L = 4 (0207 UT). F12's orbit was slightly further to the night side, moving from the 21.2 MLT meridian at L=4 (0158 UT) to the 20.3 MLT meridian at L = 1.5 (0206 UT).

We place arrows along the DMSP satellite trajectories at about 2.8 R_E to indicate the directions of the observed azimuthal velocity in Figure 4. It shows that F13 at the dayside edge of the plume measured an eastward azimuthal velocity, whereas both F12 and F15in the evening sector

measured westward azimuthal velocity. Figure 5 plots the radial profiles of equatorial azimuthal velocities deduced from DMSP horizontal velocities as a function of radial distance L, where L is determined by tracing the field line from DMSP to the equatorial plane Figure 5 also plots plasma corotation velocity equal to $2\pi L/T$ with T = 86400 s, as a straight dashed line. For consistency with the ROCSAT-1 data presentation we define the velocities to be positive in the co-rotation direction (eastward). Note that this definition is opposite to the typical convention for presenting DMSP ion drift velocities. F13 at the dayside edge of the plume observed an eastward azimuthal velocity slightly less than the co-rotation velocity for L < 2.8, where locates the outermost boundary of He^+ density along the F13 trajectory (marked by the symbol *). Outside the He^+ density boundary (L > 2.8), the equatorial azimuthal velocity along the F13 MLT decreased almost linearly with radial distance. At L = 4 the equatorial azimuthal velocity was about 30% less than the co-rotation velocity.

Both F12 and F15 detected about the same eastward equatorial azimuthal velocity as F13 at radial distance L < 2.1. According to the EUV image the He^+ plasmaspheric boundary was also at L = 2.1 in the 20-21 MLT range where F12 and F15 satellites passed through the boundary (marked by the symbol *). Beyond the He^+ plasmaspheric boundary (L > 2.1), the equatorial azimuthal velocity in the 20-21 MLT sector started to deviate substantially from the co-rotation velocity. From L=2.5 to L =3.5 the equatorial azimuthal velocity became negative, indicating strong westward flow. The peak of the westward flow reached as high as 2 km/s at L = 2.7, near the outermost boundary of the plume. The equatorial azimuthal velocity profiles observed by F12 and F15 in the evening hours are in agreement with the SAPS signatures [Foster and Vo, 2002]. The simultaneous DMSP and IMAGE observations for this event suggest strong westward component of the flow outside the He^+ density boundary in the evening sector. However the westward component of SAPS flows was absent in the F13 radial profile. This suggests that the westward component of the SAPS velocity inside L = 4 diminished between 20 and 17 MLT, before reaching the F13 MLT. By comparing the F12 and F15 velocity profiles, we estimate that at L=2.8 the SAPS azimuthal velocity decreased by a factor of 4 from between 21 and 20 MLT. Furthermore the SAPS azimuthal velocity reduction appeared to occur only for L < 3.

Another outstanding feature is the convection of equatorial plasmas toward the plume in the inertial frame. Recall that at radial distance between 2.1 to 3.5 R_E plasma azimuthal velocity was eastward (positive) before the plume MLT, and plasma azimuthal velocity after the plume MLT was westward (negative). This means the presence of a negative azimuthal gradient in equatorial

azimuthal velocity across the plume from 16.5 MLT to 20 MLT. The large azimuthal gradient was mainly confined to the radial range of SAPS with the largest gradient located at the radial distance of the outermost boundary of the plume. We emphasize that the direction of the azimuthal velocity gradient outside the He^+ density boundary ($L > 2$) was opposite to the zonal velocity gradient observed by ROCSAT-1 at lower L shells ($L < 1.5$).

4. Discussion

By using simultaneous observations from ROCSAT-1 and DMSP satellites at various magnetic local times, we obtain complimentary views of azimuthal plasmaspheric convection in the plume's neighborhood during the 16 July 2000 magnetic storm. ROCSAT-1 measurements unexpectedly indicate that the zonal velocity changes from westward to eastward at dusk. Thus at low L shells the zonal velocity observed by ROCSAT-1 has a sharp positive gradient at the plume's longitude. However, the azimuthal velocity gradient observed by DMSP satellites near the plume's outermost boundary is in the opposite direction. In the inertial frame equatorial plasmas in the outer plasmasphere convect toward the plume from both sides of the plume, suggesting a large negative azimuthal velocity gradient across the plume, mainly in the radial distance range of SAPS from 2 to 3.5 R_E.

Ion drifts measured by the ROCSAT-1 and DMSP satellites during the magnetic storm of 15 July 2000 have been investigated previously. Basu et al. [2001] reported that ROCSAT-1 detected large ion drifts in the south-westward and upward directions in the beginning of the main phase. The peak of drift velocity occurred at dusk, but no velocity reversal was seen. Lin et al. [2001] examined the ROCSAT-1 ion drift measurements during six passes throughout this storm and found large south-western flows near the South Atlantic anomaly during the main phase. During the recovery phase SAA flows have subsided. For example Figure 2 indicates a small SAA radial outward flow (V_M ~ 100 m/s) at 23 MLT away from the plume region (~ 17 MLT). Vlasov et al. [2003] also analyzed ionospheric horizontal velocity measured by the DMSP F13 and F15 satellites during this storm. They have focused on TEC enhancements during the main phase, but did not report an azimuthal-velocity reversal. Nevertheless they speculated that westward plasma flow should cease after the transition from the night to the day side. Our results support this speculation during the storm's recovery phase. Although these previous studies have investigated ROCSAT-1 ion flows during the Bastille Day storm event, they have generally

focused on ROCSAT-1 passes during the main phase and have not examined the ROCSAT-1 passes we analyzed here.

4.1 SAPS Flow

The plasmaspheric plume studied here was probably created during the main phase and, according to the EUV images, weakened gradually during the recovery phase (not shown). Simultaneous ROCSAT-1, DMSP, and IMAGE satellite observations provide new information about low-latitude convection patterns near the plasmaspheric plume. They demonstrate the existence of SAPS flow outside the He^+ plasmaspheric boundary in the evening sector on the nightside of the plume. However, DMSP F13 did not detect SAPS-like flows near the dayside edge of the plume. Our observations thus suggest the SAPS flow were diverted radially outward before reaching the plume Since the SAPS flow follows equipotentials of the total electric field, the diversion of SAPS flow implies the distortion of the convective electric field from the typical Volland-Stern model [Volland, 1973; Stern, 1975], as suggested by Goldstein et al., [2005].

Inside the plasmasphere and the plume, plasmas convect slightly slower than the co-rotation velocity (Figure 5), suggesting that the dawn-to-dusk electric field was partially shielded inside the plume during the recovery phase. Since the SAPS was detected ~ 1 R_E beyond the He+ plasmaspheric boundary, SAPS-associated plasmas flow follow equipotential lines outside the plasmaspheric boundary. Assuming that the plasma is incompressible, the $\nabla \quad \mathbf{V} = 0$ condition implies that SAPS plasma should flow along the plasmaspheric boundary in the dusk sector toward the outer, dayside magnetosphere. This could be the basis for a simple explanation for the observed radial diversion of SAPS flow.

Goldstein et al. [2005] developed a model of SAPS potential distribution in the magnetospheric equatorial plane. When compared with the Volland-Stern model, their model suggests that the SAPS flow channel significantly alters plasma streamlines in the afternoon and evening MLT sectors. We use the equipotential lines as the convection stream lines to compare their SAPS potential model with the flow directions observed by the DMSP satellites. Figure 6 shows equipotential lines of the SAPS electric potentials added to the Volland-Stern model for Kp = 7, which was selected because the Kp index decreased from 9 to 6 during the early recovery phase of the storm event. The red line indicates the zero-energy Alfven boundary (ZEAB), the outermost closed equipotentials, along which cold plasmas convect in the direction of co-

rotational (red arrows). Outside the ZEAB, the SAPS flows westward in the evening sector (yellow streams with black arrows). The flow pattern is generally consistent with the DMSP observations indicating that convection flow directions point toward the plume MLT. However, some observational details are not evident in the SAPS model of equipotential lines. For example, the major axis of the ZEAB should be rotated from the dusk toward the afternoon to account for the more pronounced plume bulge. The radial diversion of SAPS flow in the model is also not as large as expected from the observations.

Foster et al. [2002] associated Storm Enhanced Densities (SEDS) with the plasmaspheric drainage plume. Recently Kelley et al. [2004] offered a quantitative explanation for density enhancements associated with SEDS. Following their explanations, we suggest the scenario illustrated in cartoon form in Figure 7, to explain our ROCSAT-1 and DMSP observations. We project equatorial plasma flows in the vicinity of the plume into the topside ionosphere, where the plasma flow velocity is presented with co-rotational velocity subtracted. The plasmaspheric boundary is represented by a dashed line near L = 2 in the afternoon and evening sectors. The boundary extends to higher latitudes near the plume. SAPS appear as blue arrows initially flowing westward in the evening sector. Wolf [1970] showed that equipotentials pile up near the dusk terminator. As a result, zonal transport diminishes but poleward transport continues, guiding the plume toward higher latitudes.

4.2 Azimuthal Velocity Reversal

ROCSAT-1 observed the zonal velocity reversal accompanied by upward, field-aligned plasma flow. Here we attempt to examine the relationship of azimuthal gradient in zonal velocity with field-aligned flow more quantitatively. ROCSAT-1 observations of the zonal velocity V_Z changing from westward to eastward near the plume's longitude imply a large and positive divergence ($\nabla \cdot V_Z > 0$). Because ROCSAT-1 data suggest small radial velocity V_M and $V_Z \approx 0$ near the stagnation point, we express the conservation of ion density flux N as

$$\frac{\partial N}{\partial t} + N\nabla \cdot V_Z + \nabla \cdot NV_{\parallel} = 0 \qquad (8)$$

where V_{ll} is parallel velocity component along the magnetic field. At the altitudes of interest ion production and loss rates ($\partial N/\partial t$) are negligible. Since $\nabla \cdot V_Z > 0$, Equation (8) suggests that $\nabla \cdot NV_{ll} = d(NV_{ll})/ds \approx V_{ll}\,(dN/ds) < 0$ at the plume longitudes, where the symbol "s" represents distance along field lines from the equator toward the northern hemisphere. Since ion density N

along a field line is expected to increase with distance from the equator (dN/ds >0), we then obtain the condition $V_{ll} < 0$ in the northern hemisphere. By the similarly arguments, we could show that $V_{ll} > 0$ in the southern hemisphere. Therefore the zonal velocity reversal observed by ROCSAT-1 implies field-aligned ion flow from the ionospheres in both hemispheres toward the equator. These upward field-aligned flows likely carry ions from the topside ionosphere to refill the plasmaspheric plume at lower L shells. Because ROCSAT-1 detected upward field-aligned flow at 600 km altitude, sources of ions refilling the plasmasphere are probably near the F peak layer.

DMSP satellites have no measurements that allow us to determine whether field-aligned flows accompanied the azimuthal velocity reversal. However, by using the same physical arguments for interpreting ROCSAT-1 measurements, we argue that some equatorial ions probably flowed along field lines toward the ionosphere due to the azimuthal velocity reversal observed by DMSP in the radial distance range of SAPS. Since the DMSP observations indicates peak of equatorial azimuthal velocity gradient near the plume outmost boundary, the drainage plume probably lost partially some ions near the plume's outermost boundary through the field-aligned flow toward the ionosphere. The presence of field-aligned flow does not exclude or contradict with the general belief that the bulk part of SAPS ions proceeds radially outward [Foster 2004].

Figure 7 illustrates the relationship between zonal-velocity reversals and field-aligned flows. The zonal velocity reversal observed by ROCSAT-1 is represented by two oppositely pointing velocity vectors away from dusk at low latitude. The associated upward field-aligned flow from the ionosphere is represented by a red vector from the topside ionosphere along the magnetic field line (shown as dashed line) at the center of zonal velocity reversal. We also depict another field line whose foot point is near the outermost boundary of the plume (L = 3 for our event). Since the DMSP observations suggest large, equatorial azimuthal flows near the outmost boundary that point toward the plume, we display two pointing vectors at the equator toward the field line of the plume. Field-aligned flows toward the higher latitude ionosphere along the magnetic field line of the plume are illustrated by two red vectors pointing away from the equator. The plasma refilling route would follow the field line from the low latitude ionosphere to the equator, then radially outward from the low L shells to higher L shells, and finally along field lines returning to higher latitude ionosphere.

5. Conclusion

We report first observations of equatorial convection signatures associated with a plasmaspheric drainage plume using multi-satellite simultaneous observations during the recovery phase of the 2000 Bastille Day magnetic storm. These observations provide new evidence about the possible diversion of SAPS flow and the distinct signatures of azimuthal velocity reversals in the vicinity of plasmaspheric plumes. In the case of ROCSAT-1 observations at low L shells ($L < 1.5$), the zonal velocity reversal had a sharp positive velocity gradient accompanied by upward field-aligned flow. Observations of three DMSP satellites indicate an azimuthal velocity reversal with a large negative gradient across the plume in the radial distance range from 2 to 3.5 R_E. Although DMSP had no measurements of field-aligned flow, the azimuthal velocity reversal with a negative gradient suggests field-aligned flow toward the ionosphere.

The study of plasma flows in the inner magnetosphere is useful for understanding the interplay between the corotation and convection electric fields. The latter is the main force controlling the distribution of cold plasma in Earth's inner magnetosphere. Convective electric fields in the dusk sector appear to have complicated structures inside the drainage plume and outside the plasmapause where sub-auroral polarization streams flow. Further study is needed to deduce empirical models of electric fields from the observed convective velocities that would shed light on the formation of plasmaspheric boundary structures. The present work suggests that field-aligned flows within the plume play an important role in the plume formation. A better understanding of plume formation will require more modeling of plasmaspheric refilling and depletion processes.

Acknowledgements.

We are grateful for many useful discussions with Odile de La Beaujardière. The present work was supported in part by NASA SEC-GI grant NNG04GI70G and Air Force contract F19628-02-C-0012 and NSF grant ATM-0334506 with Boston College. The IMAGE program at Southwest Research Institute was sponsored by NASA Contract No. NAS5-96020, and IMAGE EUV analysis was supported through a SwRI subcontract to the University of Arizona. Magnetic field mapping algorithms used in the production of Figure 4 were developed at the MIT Haystack Observatory under support of NASA Contract No. NAG5-12875 to the Massachusetts Institute of

Technology. National Central University received support for this work from National Science Council of Taiwan through NSC grant 93-2111-M-008-011.

References

Chen, A. J., and R. A Wolf (1972), Effects on the plasmasphere of a time-varying convection electric field, Planet. Space Sci., 20, 483.

Foster, J. C., and H. B. Vo (2002), Average characteristics and activity dependence of the subauroral polarization stream, J. Geophys. Res., 107(A12), 1475, doi:10.1029/2002JA009409.

Foster, J. C., P. J. Erickson, A. J. Coster, J. Goldstein, and F. J. Rich (2002), Ionospheric signatures of plasmaspheric tails, Geophys. Res. Lett., 29(13), doi:10.1029/2002GL015067.

Foster, J. C., A. J. Coster, P. J. Erickson, F. J. Rich, and B. R. Sandel (2004), Stormtime observations of the flux of plasmaspheric ions to the dayside cusp/magnetopause. Geophys. Res. Lett., 31, L08809, doi:10.1029/2004GL020082.

Goldstein, J., B. R. Sandel, M. R. Hairston, and P. H. Reiff (2003a), Control of plasmaspheric dynamics by both convection and sub-auroral polarization stream, Geophys. Res. Lett., 30(24), 2243, dot:10.1029/2003GL018390.

Goldstein, J., M. Spasojevic, P. H. Reiff, B. R. Sandel, W. T. Forrester, D. L. Gallager, and B. W. Reinisch (2003b), Identifying the plasmapause in IMAGE EUV data using IMAGE RPI in situ steep density gradients, J. Geophys. Res., 108(A4), 1147, doi:10.1029/2002JA009475.

Goldstein, J., B. R. Sandel, M. F. Thomsen, M. Spasojevic, and P. H. Reiff (2004), Simultaneous remote sensing and in situ observations of plasmaspheric drainage plumes, J. Geophys. Res., 109, A03202 doi:10.1029/2003JA010281.

Goldstein, J., J. L. Burch, and B. R. Sandel (2005), Magnetospheric model of substorm polarization stream, J. Geophys. Res., 110, A09222, doi:10.1029/2005JA011135.

Grebowsky, J. M. (1970), Model study of plasmaspheric motion, J. Geophys. Res., 75, 4329.

Kelley, M. C., M. Vlassov, J. C. Foster, and A. J. Coster (2004), A quantitative explanation for the phenomenon known as plasmaspheric tails or storm-enhanced density, Geophys. Res. Lett., 31, L19809, doi:10.1029/2004GL020875.

Lambour, R. L., L. A. Weiss, R. C. Elphic, and M. F. Thomsen (1997), Global modeling of the plasmasphere following storm sudden commencements, J. Geophys. Res., 102, 24,351.

Lin, C. S., H.-C. Yeh, and S.-Y. Su (2001), ROCSAT-1 satellite observations of magnetic anomaly density structures during the great magnetic storm of July 15-16, 2000, Terr. Atmos. Ocean Sci., 12, 567-582.

Lin, C. S., and H.-C. Yeh (2005) Observations of electric fields associated with magnetic anomaly density structures during the July 2000 magnetic storm, Journal Geophys. Res., 110, AO03305, doi:10.1029/2003JA010215, 2005.

Mishin, E. V., W. J. Burke, C. Y. Huang, and F. J. Rich (2003), Electromagnetic wave structures within subauroral polarization streams, J. Geophys. Res., 108(A8), 1309, doi:10.1029/2002JA009793

Moldwin, M. B., B. R. Sandel, M. Thomsen, and R. Elphic (2003), Quantifying global plasmaspheric images with in situ observations, Space Sci. Rev., 109, 47-61,

Mozer, F. S. (1970), Electric field mapping in the ionosphere at the equatorial plane, Planet. Space Sci., 18, 259-263.

Sandel, B. R., R. A. King, W. T. Forrester, D. L. Gallagher, A. L. Broadfoot, and C. C. Curtis (2001), Initial results from the IMAGE Extreme Ultraviolet Imager, Geophys. Res. Lett., 28(8), 1439-1442, 2001.

Sandel, B. R., J. Goldstein, D. L. Gallagher, and M. Spasojevic (2003), Extreme ultraviolet imager observations of the structure and dynamics of the plasmasphere, Space Sci. Rev., 109, 25.

Spiro, R. W., M. Harel, R. A. Wolf, and P. H. Reiff (1981), Quantitative simulation of a magnetospheric substorm: 3, Plasmaspheric electric fields and evolution of the plasmapause, J. Geophys. Res., 86, 2261.

Stern, D. P. (1975), The motion of a proton in the equatorial magnetosphere, J. Geophys. Res., 80, 595.

Tsyganenko, N. A. (2002), A model of the near magnetosphere with a dawn-dusk asymmetry 1. Mathematical structure, J. Geophys. Res., 107(A8), 1179, doi:10.1029/2001JA000219.

Vlasov, M., M. C. Kelley, and H. Kil (2003), Analysis of ground-based and satellite observations of F-region behavior during the great magnetic storm of July 15, 2000, J. Atmos. Sol. Terr. Phys., 65, 1223-1234.

Volland, H. (1973), A semiempirical model of large-scale magnetospheric electric fields, J. Geophys. Res., 78, 171.

Wolf, R. A. (1970), Effects of ionospheric conductivity on convective flow of plasma in the magnetosphere, J. Geophys. Res., 75 (25), 4677-4698.

Weiss, L. A., R. L. Lambour, R. C. Elphic, and M. F. Thomsen (1997). Study of plasmaspheric evolution using geosynchronous observations and global modeling, Geophys. Res. Lett., 24, 599.

Yeh, H.-C., Su, S. Y., Yeh, Y. C., Wu, J. M., Heelis, R. A., and Holt, B. J. (1999), Scientific mission of the IPEI payload on board ROCSAT-1, TAO supplementary issue, 10, 19-42.

Figure Captions

Figure 1. (1a) EUV image of a plasmaspheric plume taken by the IMAGE satellite at 0132 UT and (1b) convective velocity vectors on the equatorial plane measured by ROCSAT-1 during one complete orbit from 0040 UT to 0216 UT on 16 July 2000. The dark circles in Figure 1b mark the position of the He^+ plasmaspheric boundary determined from the EUV image. Line A corresponds to the location where the He^+ plasmaspheric boundary starts to bulge, Line B marks the plume's dayside edge, and Line C marks the nightside edge of the plume. The velocity vectors in Earth's co-rotating frame of reference are plotted as red vectors at every half hour in MLT. The dotted circles at radial distance 3 and 4 R_E are plotted for coordinate reference. A vector with the length equal to 300 m/s is shown as a scale for the velocity vectors.

Figure 2. Convective velocities and field-aligned velocity deduced from ROCSAT-1 data as a function of MLT. The top panel shows the zonal velocity component V_Z, the second panel plots the radial velocity component V_M, and the third panel plots the field-aligned velocity. Convective velocities measured at the ROCSAT-1 altitude (600 km) are presented in blue; equatorial convective velocities are in red. The satellite geomagnetic latitude is plotted in the bottom panel. Vertical lines A, B, and C correspond to three radial lines shown in Figure 1b.

Figure 3. Equatorial zonal velocity in Earth's inertial frame (top panel) and L value (bottom panel) as a function of MLT for one ROCSAT-1 orbit. The horizontal curve is the corotation velocity in the equatorial plane for the given L. Vertical dashed lines A, B, and C are defined the same as Figure 2.

Figure 4. EUV image of the He^+ plasmasphere mapped to the equatorial plane in GSM coordinates. Trajectories of three DMSP satellites F12, F13, and F15 are mapped to the equatorial plane and overlaid on the EUV image. Arrows on the DMSP satellite tracks indicate directions of the observed convection.

Figure 5. Radial profiles of the equatorial azimuthal velocity deduced from DMSP ion drift data near 0200 UT on day198, 16 July 2000, with F13 at 16.3 MLT (blue solid line), F15 at 20.6 MLT (red dotted line), and F12 at 21 MLT (red dashed line). The straight dashed line represents the co-rotational velocity. The azimuthal velocity is positive in the corotation (eastward) direction.

Large negative (westward) azimuthal flow is due to SAPS. The locations of the He^+ plasmaspheric boundary are marked by the * symbol on the radial profiles of azimuthal velocity for each satellite.

Figure 6. Equatorial magnetospheric SAPS potential model for Kp = 7. In the plot, the Earth is in the center, and the sun is to the right. The SAPS potentials are produced using the SAPS potential model of Goldstein et al. [2005]. The red line represents the zero-energy Alfven boundary. SAPS plasmas flow westward in the evening hours are presented by black arrows.

Figure 7. Scenario of plasma convection and field-aligned flows in the vicinity of the plasmaspheric drainage plume. The schematic of convection flows at the topside ionosphere is inferred from the convection patterns on the magnetosphere equatorial plane.

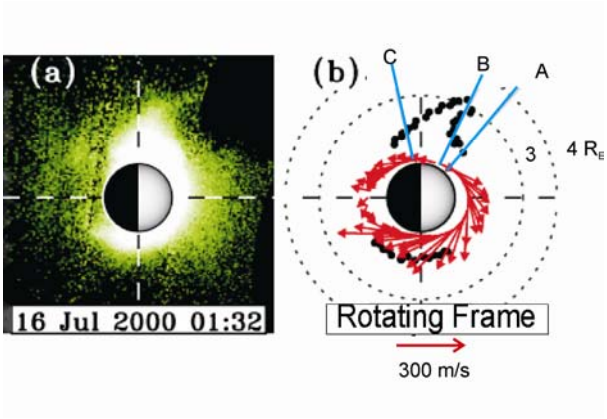

Figure 1

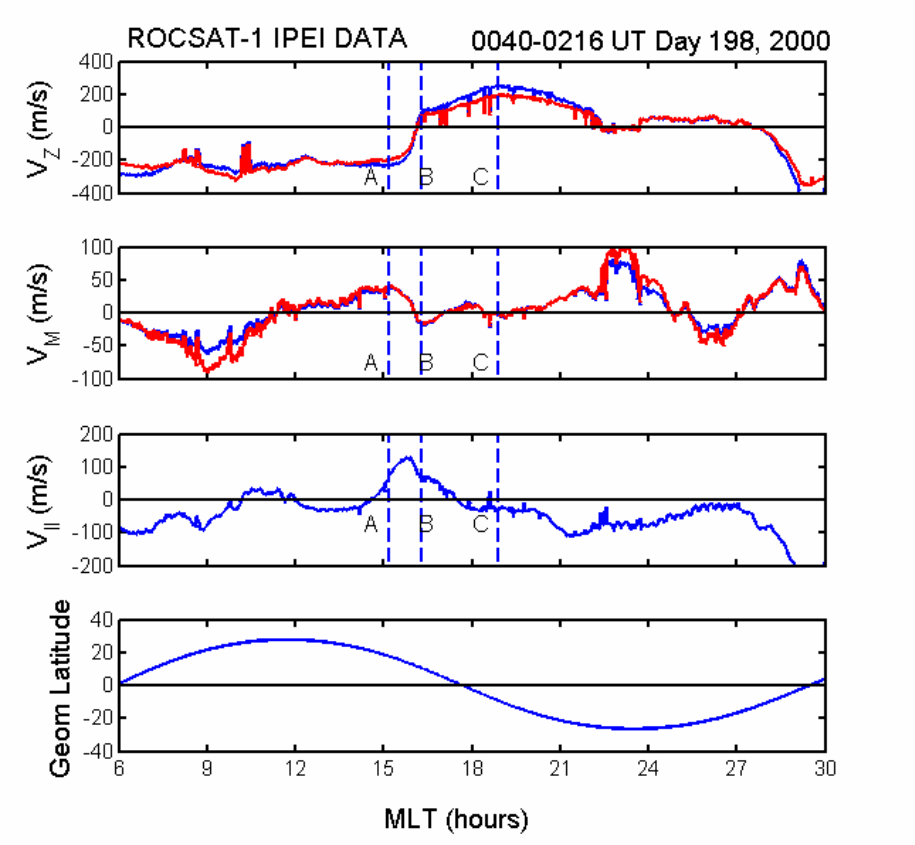
ROCSAT-1 IPEI DATA
0040-0216 UT Day 198, 2000
V_Z (m/s)
V_M (m/s)
$V_{||}$ (m/s)
Geom Latitude
A
B
C
MLT (hours)

Figure 2

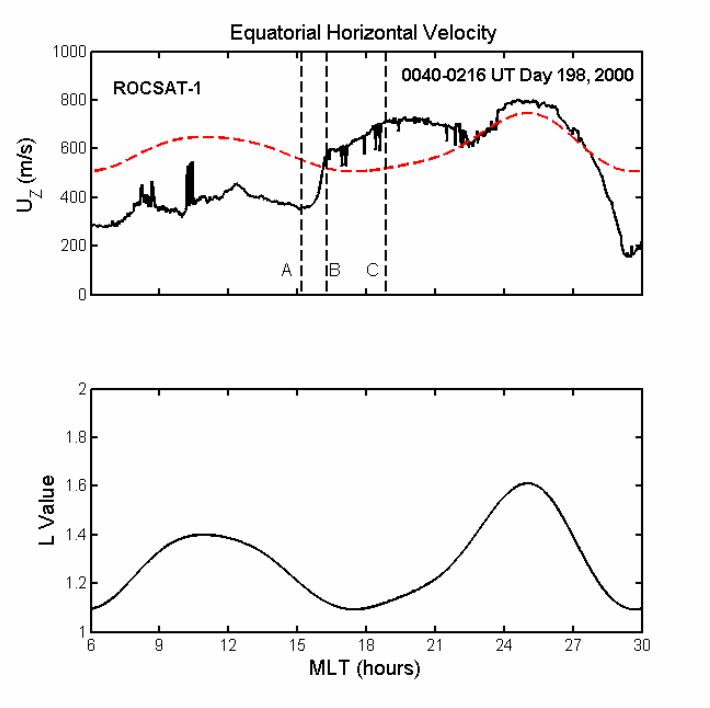
Equatorial Horizontal Velocity
ROCSAT-1
0040-0216 UT Day 198, 2000
U_Z (m/s)
1000
800
600
400
200
0
A
B
C
L Value
2
1.8
1.6
1.4
1.2
1
6
9
12
15
18
21
24
27
30
MLT (hours)

Figure 3

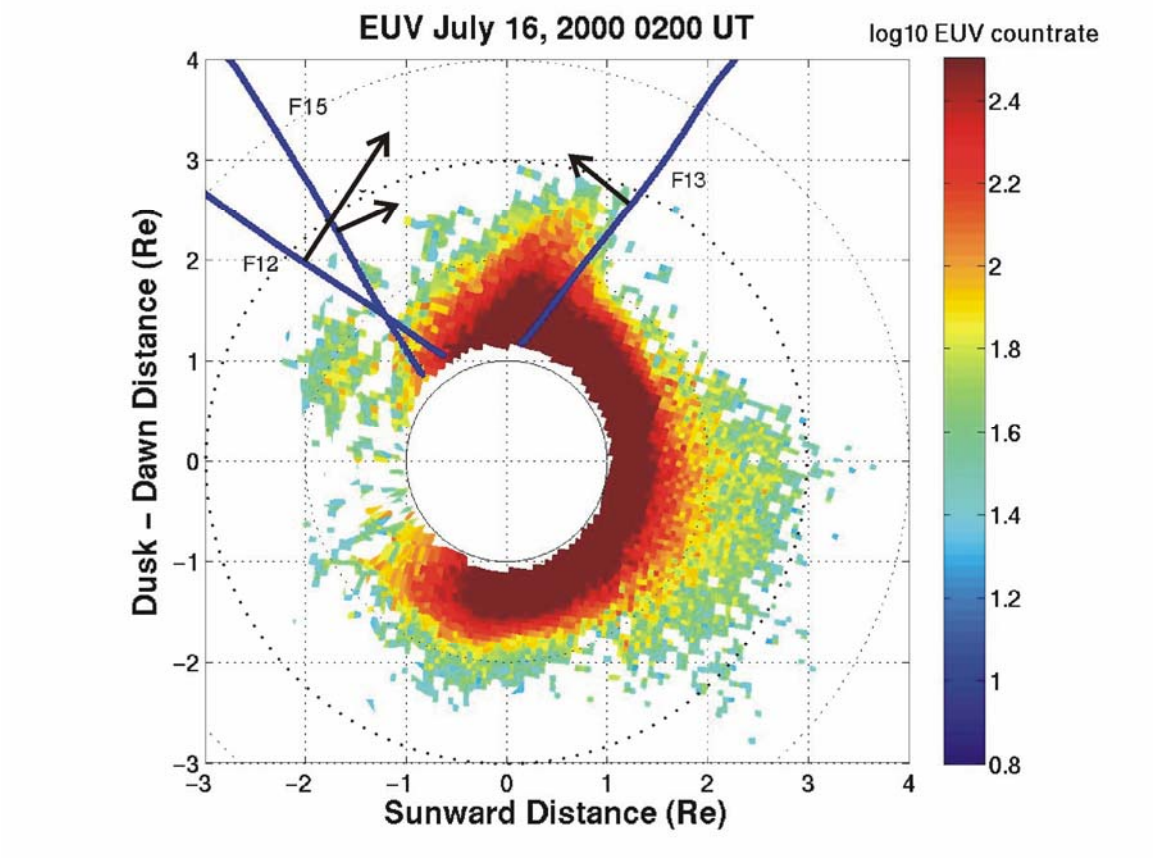
EUV July 16, 2000 0200 UT
log10 EUV countrate
F15
F13
F12
Dusk – Dawn Distance (Re)
Sunward Distance (Re)
4
3
2
1
0
−1
−2
−3
2.4
2.2
2
1.8
1.6
1.4
1.2
1
0.8

Figure 4

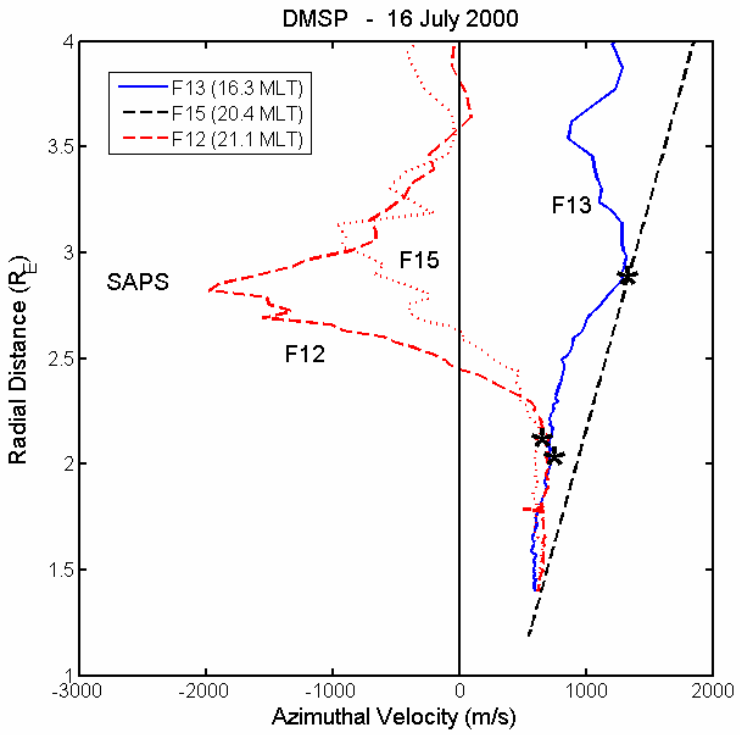
DMSP - 16 July 2000
F13 (16.3 MLT)
F15 (20.4 MLT)
F12 (21.1 MLT)
SAPS
F12
F15
F13
Radial Distance (R_E)
Azimuthal Velocity (m/s)
4
3.5
3
2.5
2
1.5
1
-3000
-2000
-1000
0
1000
2000

Figure 5

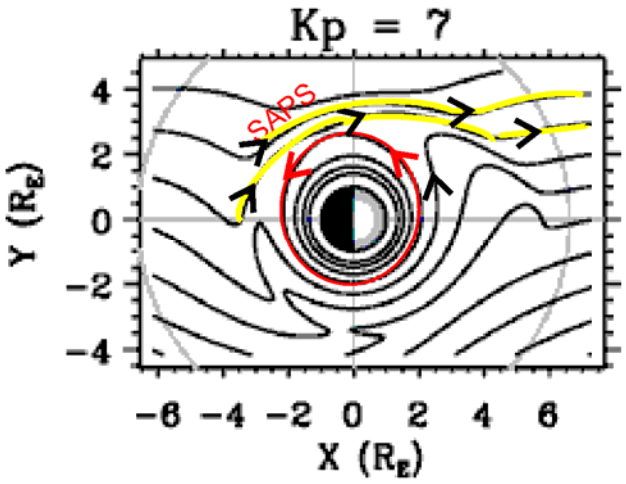

Figure 6

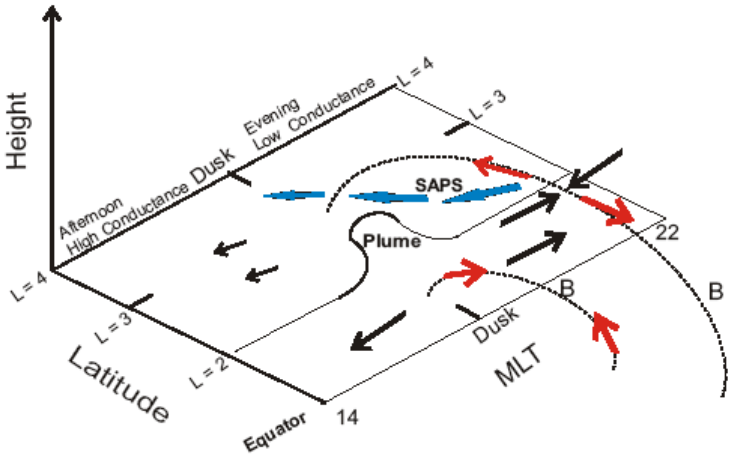
Height
Afternoon
High Conductance
Dusk
Evening
Low Conductance
L = 4
L = 3
SAPS
Plume
22
B
B
L = 4
L = 3
L = 2
Latitude
Equator
14
Dusk
MLT

Figure 7